Nano Research
2023, 16(3): 4093–4099

ISSN 1998-0124 CN 11-5974/O4
https://doi.org/10.1007/s12274-022-5162-0

Research Article

Ultra-sensitive and wide applicable strain sensor enabled by carbon nanofibers with dual alignment for human machine interfaces

Peng Bi[1,2], Mingchao Zhang[1], Shuo Li[1], Haojie Lu[1], Haomin Wang[1], Xiaoping Liang[1], Huarun Liang[1], and Yingying Zhang[1,2] (✉)

[1] *Key Laboratory of Organic Optoelectronics and Molecular Engineering of the Ministry of Education, Department of Chemistry, Tsinghua University, Beijing 100084, China*
[2] *Laboratory of Flexible Electronics Technology, Tsinghua University, Beijing 100084, China*

Received: 29 August 2022 / **Revised:** 30 September 2022 / **Accepted:** 7 October 2022

ABSTRACT

Flexible strain sensors with high sensitivity, wide detection range, and low detection limit have continuously attracted great interest due to their tremendous application potential in areas such as health/medical-care, human–machine interface, as well as safety and security. While both of a high sensitivity and a wide working range are desired key parameters for a strain sensor, they are usually contrary to each other to be achieved on the same sensor due to the tightly structure dependence of both of them. Here, a flexible strain sensor with both high sensitivity and wide strain detection range is prepared based on the design of an integrated membrane containing both of parallel aligned and randomly aligned carbon nanofibers (CNFs). The parallel aligned CNF membrane (p-CNF) exhibits a low strain detection limit and high sensitivity, while the random aligned CNF membrane (r-CNF) exhibits a large strain detection range. Taking the advantages of both p-CNF and r-CNF, the strain sensor with stacked p-CNF and r-CNF (p/r-CNF) exhibits both high sensitivity and wide working range. Its gauge factor (GF) is 1,272 for strains under 0.5% and 2,266 for strain from 70% to 100%. At the same time, it can work in a wide strain range of 0.005% to 100%, fulfilling the requirements for accurately detecting full-range human motions. We demonstrated its applications in the recognition of facial expressions and joint movements. Furtherly, we constructed an intelligent lip-language recognition system, which can accurately track phonetic symbols and may help people with language disabilities, proving the potential of this strain sensor in health management and medical assistance. Besides, we foresee that the dual-alignment structure design of the p/r-CNF strain sensor may also be applied in the design of other high performance sensors.

KEYWORDS

nanofiber membrane, carbon nanofibers, flexible sensor, dual-alignment, high sensitivity

1 Introduction

In recent years, flexible wearable electronic devices have shown great application potential in the fields of action recognition [1–3], personalized health monitoring [4–6], and human–machine interaction [7–9], which are attracting extensive attention. Particularly, flexible strain sensors are a class of highly deformable sensing devices that can monitor a variety of human motions and physiological signals [10–12]. They typically consist of elastomers combined with conductive materials, such as graphene [13], carbon nanotubes [14], carbon black [15], metal nanoparticles [16], metal nanowires [17], ionic liquids [18], liquid metals [19], and conductive polymers [20]. Unlike conventional rigid sensors made of bulky metal, these flexible sensors show merits of good stretchability and conformability, lightweight as well as human friendliness. They can be integrated into clothes or directly attach to human skin.

Currently, most of the reported wearable strain sensors showed either large workable strain range or high sensitivity [21–23]. For example, a flexible strain sensor fabricated by coating super-aligned carbon nanotube membranes on polydimethylsiloxane substrates could be stretched by over 400%, but the gauge factor (GF) value of the sensor, which is an indicator of the sensitivity, is less than 0.2 [24]. Although the strain sensor has a large strain detection range, its low sensitivity limits its ability to detect small deformations. To solve the problem of low sensitivity, the strain sensor can be improved by adjusting the deformation mechanism of conductive nanomaterials, such as slip, crack propagation, and contact separation of conductive media. For instance, a strain sensor based on contact separation of anisotropic resistive structure was prepared [21]. The GF of this sensor is more than 8,500. Although it has ultra-high sensitivity, its maximum strain detection limit is only 5%. The flexible sensor based conductive medium separation mechanism will become insulating under large strain, limiting their wide applications.

It is highly desired to obtain high-performance strain sensors with both high sensibility and wide sensing range, especially for applications in accuracy monitoring full-scale human activities [25, 26]. However, in order to achieve high sensitivity, the conductivity of the microstructure sensing layer should change significantly under small deformation. Differently, to achieve wide sensing range, the sensing layer should be continuously

Address correspondence to yingyingzhang@tsinghua.edu.cn

conductive even under large tensile strain, making it difficult to simultaneously achieve high sensitivity and wide strain detection range, especially for sensors composed of a single conductive medium.

Herein, we report a flexible strain sensor with combined high sensitivity and wide strain detection range, which is achieved by using stacked parallel aligned carbon nanofiber (p-CNF) membranes and randomly aligned carbon nanofiber (r-CNF) membranes as the active materials. Both of the membranes were made from electrospinning polyamide acid nanofibers through high temperature carbonization and the orientation of the fibers in the membranes was controlled by the electrospinning process. Remarkably, the obtained p/r-CNF-based strain sensor showed a low strain detection limit as small as 0.005% and an ultra-high GF of up to 1,272. At the same time, its maximum strain detection limit is 100%, fulfilling the requirements for detection of most human motions. We demonstrated that the sensor can accurately distinguish large motions such as joint bending and minor motions such as facial expression, eye rotation, pulse, and speaking. As proof of concept, we developed an intelligent lip-language recognition system by integrating p/r-CNF strain sensors, Arduino, and a loudspeaker together, which can accurately identify the phonetic symbols of the language according to the deformation of lips, and then make corresponding instructions, such as output audio signals or turn on the light. This intelligent lip-language recognition system may help people with voice disorder.

2 Results and discussion

The p/r-CNF strain sensor consists of two CNF membranes with different orientations as sensing materials. Figure 1(a) illustrates the preparation process of p/r-CNF strain sensors. The CNF membranes were prepared by electrospinning polyamide acid (PAA) following by imidization and high temperature carbonization. A cage collector and a plate collector were used for the preparation of p-CNF and r-CNF, respectively. The electrospinning polyamide acid nanofibers were transformed into CNF membranes with good electrical conductivity through the carbonization process. Raman spectra of the membranes indicate the formation of graphite microcrystals after the carbonization process (Fig. S1 in the Electronic Supplementary Material (ESM)). As shown in Fig. 1(b), the electrospinning nanofibers collected by the cage collector are arranged in a parallel array, which is determined by the electric field distribution between the needle and the collector during electrospinning. The parallel polyamide acid nanofiber membrane was carbonized at 900 °C for 4 h in argon atmosphere and the obtained p-CNF membrane shows a resistance of 5 kΩ (Fig. S2 in the ESM). In contrast, Fig. 1(c) shows the scanning electron microscopy (SEM) image of the membrane collected by the plate collector, which is composed of randomly aligned nanofibers and can be carbonized into the r-CNF membrane. A p-CNF membrane and a r-CNF membrane were stacked together and encapsulated with polydimethylsiloxane (PDMS) to obtain a p/r-CNF-based flexible strain sensor. Figure 1(d) shows the image of the p/r-CNF strain sensor, which possesses good flexibility. The thickness of the sensor is about 0.4 mm.

Firstly, we studied the influence of nanofiber alignment on the performance of strain sensors. We prepared strain sensors using a p-CNF membrane and a r-CNF membrane, respectively. They showed different morphology evolution and electrical response under stretching. As shown in Fig. 2(a), the p-CNF membrane will show parallel cracks in the stretching process. The cracks increase with the increase of tensile strain, leading to a sharp increase in the resistance over a small strain range. The minimum strain detected by the sensor is 0.005%, corresponding to the sensor's length variable of 1 μm (the length of the strain sensor is 2 cm). Such ultra-low strain detection limit can be ascribed to the obvious change of resistance caused by the appearance of parallel cracks even under ultra-low strain. When the strain changes from 0.005% to 0.05%, the relative change in resistance also increases from 0.01% to 0.46% (Fig. 2(b)). Furtherly, as the strain changes from 0.05% to 0.5%, the crack becomes larger and longer, leading to more than 10 times increase in the variation of resistance (Fig. 2(c)). It should be noted that if the strain continues to be increased, the current will approach 0 (Fig. S3 in the ESM), losing the detection ability for strain. In contrast, the flexible sensor fabricated based on the r-CNF shows a detectable strain range over 100%. The r-CNF membrane can also change in shape under

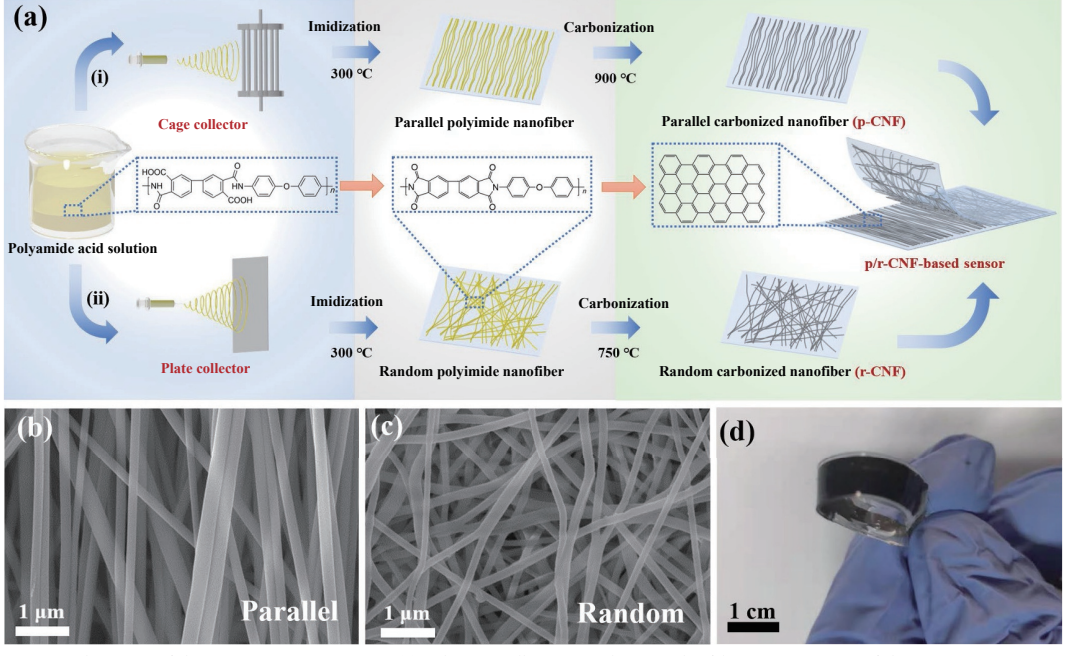

Figure 1 Preparation and images of the p/r-CNF strain sensor. (a) Schematic illustration showing the fabrication process of the p/r-CNF strain sensor. (b) and (c) SEM images of p-CNF (b) and r-CNF (c). (d) Photograph of a p/r-CNF-based flexible strain sensor.

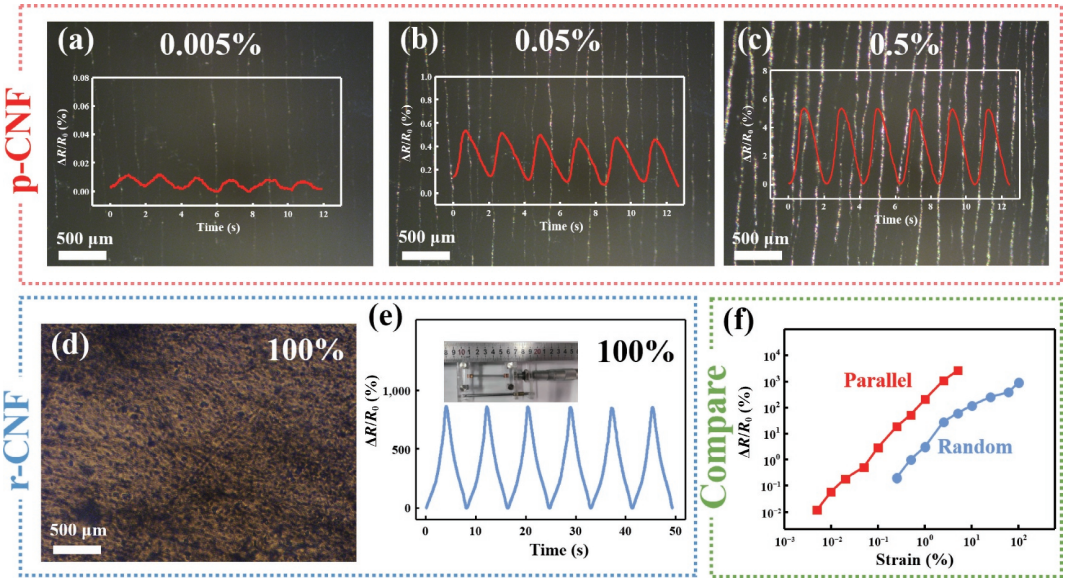

Figure 2 Comparison of structure evolution and strain sensing performance of p-CNF and r-CNF based strain sensors. (a)–(c) Optical images and relative resistance change of p-CNF membranes induced by cycling loading-unloading of 0.005% (a), 0.05% (b), and 0.5% (c) strain. (d) Optical image of a r-CNF membrane under 100% strain showing no cracks on the surface. (e) Relative resistance change of r-CNF based strain sensor induced by cycling loading-unloading of 100% strain. (f) Relative resistance change of p-CNF and r-CNF based strain sensor under different strains.

stretching, but no cracks will appear. Even if the strain increases to 100%, there is still no crack observed (Fig. 2(d)). We surmise that although breaks will form along the nanofibers during stretching, the location of the fractures will be different since the nanofibers are randomly aligned. Therefore, there are no macroscopic fractures which can be observed with optical microscope. The r-CNF sensor can accurately perceive the corresponding length variables within a large strain range (Fig. 2(e)).

We compared the strain detection range and sensitivity of strain sensors based on p-CNF and r-CNF (Fig. 2(f)). It can be observed that the sensor with p-CNF as the sensing material has a high resistance variation and an extremely low strain detection limit (0.005%). However, its maximum strain detection value is only about 5%. Differently, the sensor based on r-CNF has a minimum detectable strain of 0.2% and a maximum detectable strain over 100%. Therefore, one can suppose that if these two kinds of sensing materials are combined to produce a dual-orientation CNF based strain sensor, it may simultaneously possess high sensitivity and wide strain detection range.

Figure 3(a) shows the equivalent circuit diagram of the combined p/r-CNF membrane. The total resistance of p/r-CNF membrane can be obtained from the following equation

$$\frac{1}{R_{tal}} = \frac{1}{2r_1 + r_2} + \frac{1}{R_r}$$

where r_1, r_2, and R are the resistances of the island, suspended bundle, and random nanofiber membrane, respectively. R_{tal} is the total resistance value. In our previous work [27], the resistance variation of the crack deformation mechanism is discussed. In order to optimize the sensitivity of the p/r-CNF sensor in the whole detection range, the resistance of p-CNF and r-CNF was regulated through tuning the temperature during carbonization. For the p-CNF membrane, the carbonization was carried out at 900 °C, leading to an intrinsic resistance only about 5 kΩ. In contrast, the r-CNF membrane was treated at 750 °C and its resistance is about 330 kΩ (Fig. S2 in the ESM). For the p/r-CNF flexible strain sensor, the resistance variation for resistance in the range of 5 to 330 kΩ is mainly caused by the crack generation in the p-CNF membrane induced by the applied strain which is less than 5%. The sensor shows ultra-high sensitivity in this range. When the strain is greater than 5%, the cracks become larger, and completely isolated islands form, resulting in the break of the conductive path. Therefore, the r-CNF membrane will act as the only conductive path while the applied strain is high.

The p/r-CNF flexible strain sensor can not only sensitively perceive small strains (Fig. 3(b)), but also detect large strains (Fig. 3(c)) with high reliability. The sensing performance of the p/r-CNF strain sensor was investigated by monitoring the relative resistance change ($\Delta R/R_0$, where $\Delta R = R - R_0$, R_0 and R are the resistances of the strain sensor before and after stretching, respectively) at different strains (ε). The sensitivity can be evaluated using the GF value (GF = $(R - R_0)/\varepsilon$) [28]. Figure 3(d) shows the relative resistance change of the p/r-CNF strain sensor for strain in the range of 0% to 100%. The elongation at break of p/r-CNF strain sensor is 116% (Fig. S4 in the ESM). The GF was calculated to be 1,272 for strains under 0.5% and 2,266 for strains from 70% to 100%, indicating the p/r-CNF strain sensor has ultra-high sensitivity for both low and high strains. The ultra-high GF value in the low strain range is mainly related to the parallel aligned fiber structure of p-CNF membrane. A small change in strain can cause a sharp change in resistance. In the large strain range, the rapid increase of resistance with increasing strain is mainly caused by the fracture of r-CNF nanofibers. Remarkably, the low strain detection limit of the strain sensor can be down to as low as 0.005%. Compared with previous reports [24, 28–39], the p/r-CNF strain sensor has wide strain detection range and high sensitivity for the whole strain detection range (Fig. 3(e)). Besides, the sensor shows high stability. It maintained repeatable response to cyclic loading and unloading of 80% strain for 4,000 cycles (Fig. 3(f)). At the same time, it possesses fast response ability to strain and the response time is less than 100 ms (Fig. S5 in the ESM).

Due to the wide strain detection range and high sensitivity of the p/r-CNF strain sensor, it can be used for full-scale human motion monitoring. As illustrated in Fig. 4(a), the strain sensor can be attached on human body to track movement of joints such as elbows, knees, larynx, and wrists. It can realize the detection of periodic deformation of elbow and knee induced by running (Figs. 4(b) and 4(c)). Moreover, the flexible sensor also can detect small deformations induced by pulse and speaking. As seen in Fig. 4(d), the intensity of pulse signal after exercise is more than twice that before exercise. As shown in Fig. 4(e), recognition of words can be

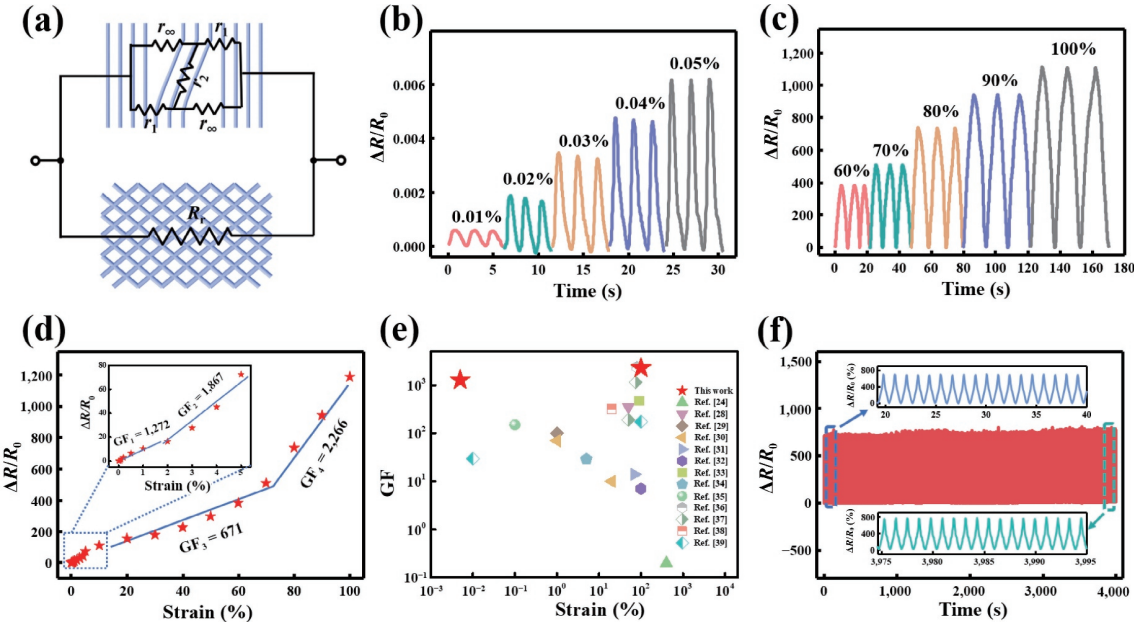

Figure 3 Sensing performance of the p/r-CNF strain sensor. (a) Equivalent circuit diagram of the combined p/r-CNF membrane. (b) and (c) The relative resistance change of sensor induced by small (b) and large (c) strains, showing its good reliability. (d) The relative resistance change of the sensor induced by strain, showing the GF for different strain ranges. The inset shows a magnified part of the plot. (e) Comparison of the GF and the corresponding sensing range of p/r-CNF strain sensor with those of the counterparts reported in the literatures. (f) Resistance change during 4,000 cycles of strain deformation with maximum strain of 80%, showing the cycle stability of the p/r-CNF strain sensor.

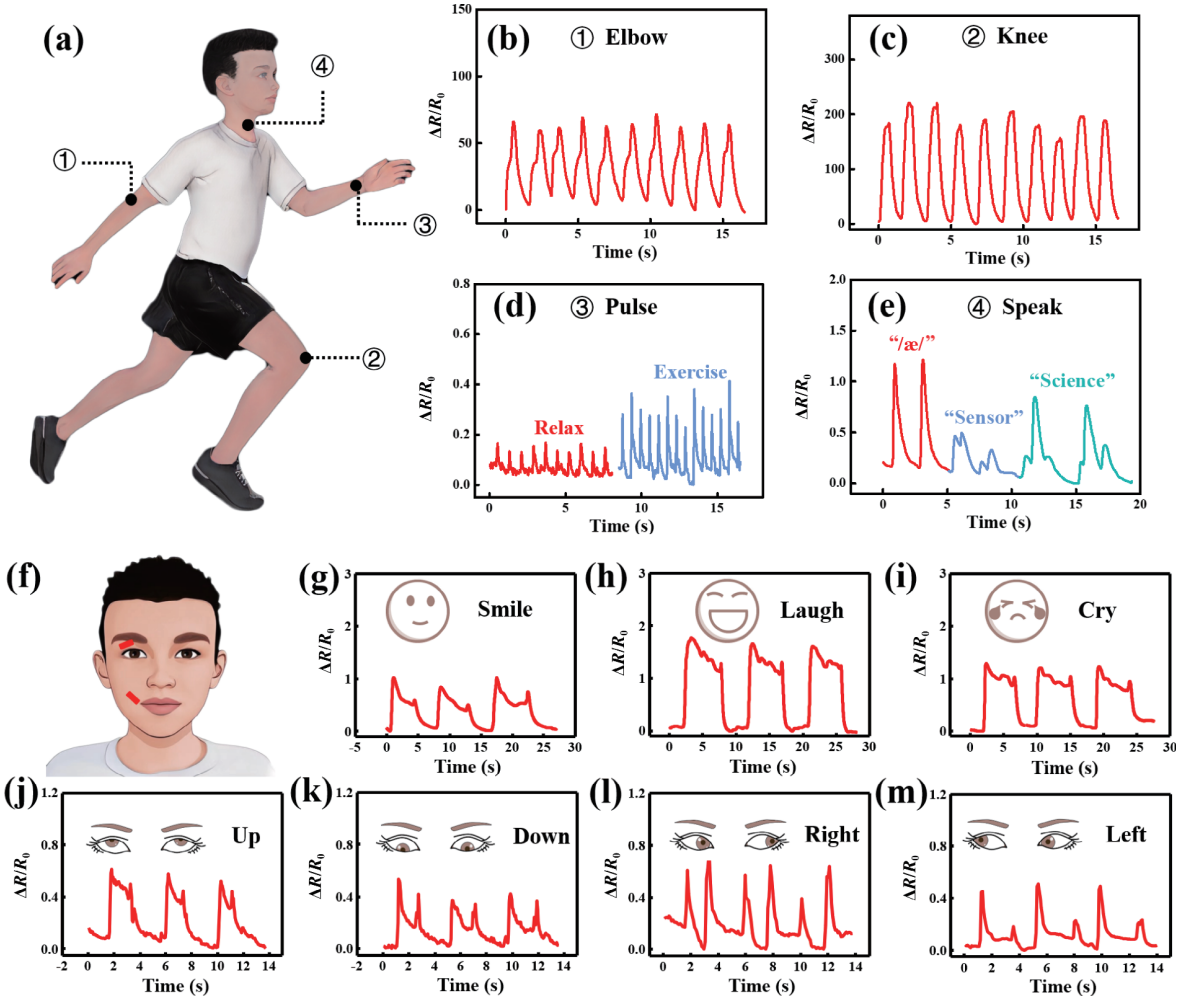

Figure 4 Potential applications of the p/r-CNF strain sensor in detection of joint motions and facial expressions. (a) Illustration showing the location of the sensors for motion detection. (b) and(c) Relative resistance change induced by motion of elbow (b) and knee (c) during running. (d) Relative resistance change induced by pulse before and after exercise. (e) Relative resistance change induced by speaking. (f) Schematic illustration showing the location of sensors on the cheek and upper eyelid to monitor facial expressions and eye movements. (g)–(i) Relative resistance change induced by smiling (g), laughing (h), and crying (i). (j)–(m) Relative resistance change induced by eye movements of looking up (j), down (k), right (l), and left (m).

realized by attaching a sensor on throat to detect the vibration induced by speaking. The above results indicate that the p/r-CNF strain sensor is capable to realize the accurate detection of full-scale human motion.

Besides, we demonstrated the applications of the sensor in monitoring of facial expressions. As can be seen from Figs. 4(f)–4(i), the sensor can be attached on the cheek and different signals can be obtained when a person smiles, laughs, or cries. The sensor can also be used to detect eye movement by attaching it onto the upper eyelid. When the person looks upward, downward, left, and right, the movement of eyeball can be tracked and distinguished (Figs. 4(j)–4(m)).

As this flexible sensor can sense and distinguish facial expression, it can be applied in the field of medical assistance. For example, some persons have damaged vocal cords and cannot make sound. In this case, the mouth shape can be monitored by the sensors and the obtained signals can be used for communication or other purposes. As a single sensor can only obtain simple information and is difficult to realize recognition, multiple flexible sensors can be attached onto different locations and the signals can be analyzed together in order to obtain accurate information. As proof of concept, we designed and fabricated a lip-language recognition system by integrating three p/r-CNF strain sensors, an Arduino, and a loudspeaker (Fig. 5(a)). Three sensors are attached to the upper lip, the corners of the mouth, and the cheeks, respectively, using medical tapes. The sensors will produce electronic signals when the person is speaking, which can be further processed by the Arduino which acts as the central control unit. Then, the corresponding command is output from the Arduino to the loudspeaker or other devices such as a smart light. As shown in Fig. 5(b), the sensors generate different signal combinations when the people speak different vowel phonetics, and its accuracy is very high (Fig. S6 in the ESM). In this case, the volunteer only moves lips without making a sound (Movie ESM1). The sensors can accurately identify the skin deformation and transmit this information to the Arduino in the form of voltage change. The Arduino can further control the loudspeaker or other devices. For example, the lip-language recognition system can connect to a smart light and then the light can be controlled by lip-saying "turn on" or "turn off" (Fig. 5(c) and Movie ESM2). Here, firstly, the phonetic symbol of "turn" is identified through Arduino, and then the number of phonetic symbols is counted. If the number of phonetic symbols is 2, it is "turn on", and if the number of phonetic symbols is 3, it is "turn off". Apparently, this lip-language recognition system can help people with speech disabilities to recover their daily communication as close as possible to the normal state.

3 Conclusions

In summary, we fabricated a flexible sensor with both of high sensitivity and wide strain detection range and based on combined p-CNF and r-CNF membranes. The dependence of the sensing performance on the orientation of the nanofibers in the membranes was studied and the mechanism was discussed. We found that the p-CNF shows a high sensitivity but a small workable strain range while the r-CNF can work in a wide strain range, indicating their combination may lead to both of high sensitivity and wide workable strain range. Based on this strategy, we successfully fabricated a p/r-CNF based strain sensor, which possesses high sensitivity across a wide working strain range of 0.005%–100%. For instance, its GF is 1,272 and 2,266 for strains lower than 0.5% and higher than 70%, respectively, superior to most of the reported flexible strain sensors. Based on its excellent performance, the p/r-CNF based strain sensor can detect tiny deformations in facial skin and monitor eye movements. Meanwhile, it can detect large strains induced by running and cycling, without damaging the device. As a proof of concept, we constructed a lip-language recognition system using microcontroller and p/r-CNF sensors, which can accurately distinguish phonetic symbols and control intelligent devices and thus help people with language disabilities. We believe that the development of this kind of highly sensitive and wide applicable flexible sensors will contribute to the practical applications of wearable electronics in health management, medical assistance, and human-machine interfaces.

4 Experimental

4.1 Preparation of polyimide (PI) nanofiber membranes

First, 4,4'-diaminodiphenyl ether was dissolved in N,N'-dimethylacetamide in a 250 mL two-mouth bottle, and argon was pumped as a protective gas. Next, 3,3',4,4'-biphenyl tetracarboxylic

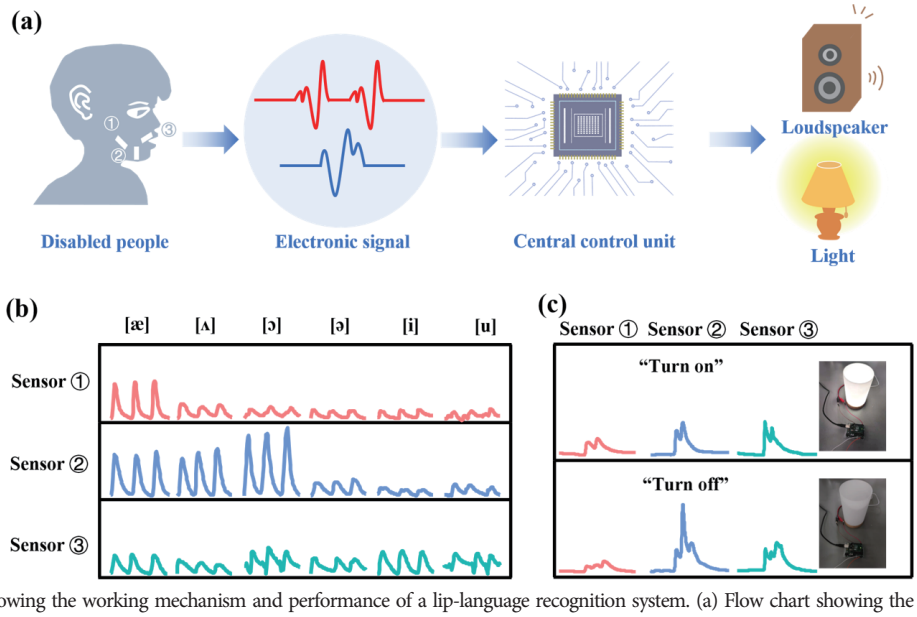

Figure 5 Illustration showing the working mechanism and performance of a lip-language recognition system. (a) Flow chart showing the working mechanism. (b) Signals of the three sensors integrated in the lip-language recognition system while the person speaks different vowel symbols. (c) Signals of the three sensors when the volunteer says "turn on" or "turn off" to control the light.

diandhydride was added in four batches and stirred thoroughly for 4 h to produce a viscous polyamide acid solution. Then, electrospinning was carried out using the obtained PAA solution. The positive and negative voltages were set to be 18 and −3 kV, respectively. The flow rate of the propulsion pump was 0.1 mm/min. The size of the nozzle was 0.33 mm. The distance from the nozzle to the receiving plate was 20 cm. Parallel aligned and randomly aligned PI membranes were collected by a cage collector and a flat plate, respectively.

4.2 Carbonized nanofiber membranes and device encapsulation

The collected PI membrane was dried at 60 °C for 6 h to remove the organic solvent in the membrane. Then, the membrane was pressed with a glass sheet and imidized at 300 °C. After that, the membrane was placed on an iron substrate and heated at 500 °C for 1 h, following by cooling down and being separated from the substrate. Then, the membrane was sandwiched between two iron sheets for high-temperature carbonization. All the above thermal treatment was carried out with a tubular furnace filled with argon. The details of the carbonization process of electrospinning membranes can be found in our previous work [40, 41]. The carbonization temperatures for the p-CNF and r-CNF were optimized and set to 900 and 750 °C, respectively, in order to obtain the desired performance. To fabricate the sensor, p-CNF membrane was first placed on a PDMS substrate, then coated with uncured PDMS, heated for 1 h, and then a r-CNF membrane was placed on. Next, the composite membrane was encapsulated using PDMS to get the flexible strain sensor. The electrodes were attached with the sensor using stretchable glue to ensure good mechanical stability.

4.3 Characterization

The morphologies of the pristine nanofibers were characterized using field-emission scanning electron microscopy (FE-SEM, FEG 450, Quanta). The loading of the tensile strain and the measurement of the stress–strain curve were performed with a universal testing machine (AGS-X, Shimadzu). The electrical signals were recorded using an electrochemical workstation (CHI 660E) and a wireless digital source meter (LinkZill-01RC). Raman spectra were recorded at room temperature using a 532 nm laser (HORIBA Evolution).

Acknowledgements

This work was supported by the National Natural Science Foundation of China (Nos. 52125201 and 21975141) and the National Key Research and Development Program of China (No. 2020YFA0210702).

Electronic Supplementary Material: Supplementary material (Raman spectra, electrical and mechanical curves, confusion matrix, and movies) is available in the online version of this article at https://doi.org/10.1007/s12274-022-5162-0.

References

[1] Wang, S. H.; Xu, J.; Wang, W. C.; Wang, G. J. N.; Rastak, R.; Molina-Lopez, F.; Chung, J. W.; Niu, S. M.; Feig, V. R.; Lopez, J. et al. Skin electronics from scalable fabrication of an intrinsically stretchable transistor array. *Nature* **2018**, *555*, 83–88.

[2] Liu, S. Q.; Zhang, J. C.; Zhang, Y. Z.; Zhu, R. A wearable motion capture device able to detect dynamic motion of human limbs. *Nat. Commun.* **2020**, *11*, 5615.

[3] Wu, Q.; Qiao, Y. C.; Guo, R.; Naveed, S.; Hirtz, T.; Li, X. S.; Fu, Y. X.; Wei, Y. H.; Deng, G.; Yang, Y. et al. Triode-mimicking graphene pressure sensor with positive resistance variation for physiology and motion monitoring. *ACS Nano* **2020**, *14*, 10104–10114.

[4] Wang, Z. Y.; Shin, J.; Park, J. H.; Lee, H.; Kim, D. H.; Liu, H. F. Engineering materials for electrochemical sweat sensing. *Adv. Funct. Mater.* **2021**, *31*, 2008130.

[5] Lin, Y. J.; Bariya, M.; Nyein, H. Y. Y.; Kivimäki, L.; Uusitalo, S.; Jansson, E.; Ji, W. B.; Yuan, Z.; Happonen, T.; Liedert, C. et al. Porous enzymatic membrane for nanotextured glucose sweat sensors with high stability toward reliable noninvasive health monitoring. *Adv. Funct. Mater.* **2019**, *29*, 1902521.

[6] Yeon, H.; Lee, H.; Kim, Y.; Lee, D.; Lee, Y.; Lee, J. S.; Shin, J.; Choi, C.; Kang, J. H.; Suh, J. M. et al. Long-term reliable physical health monitoring by sweat pore-inspired perforated electronic skins. *Sci. Adv.* **2021**, *7*, eabg8459.

[7] Jung, Y. H.; Hong, S. K.; Wang, H. S.; Han, J. H.; Pham, T. X.; Park, H.; Kim, J.; Kang, S.; Yoo, C. D.; Lee, K. J. Flexible piezoelectric acoustic sensors and machine learning for speech processing. *Adv. Mater.* **2020**, *32*, 1904020.

[8] Lim, S.; Son, D.; Kim, J.; Lee, Y. B.; Song, J. K.; Choi, S.; Lee, D. J.; Kim, J. H.; Lee, M.; Hyeon, T. et al. Transparent and stretchable interactive human machine interface based on patterned graphene heterostructures. *Adv. Funct. Mater.* **2015**, *25*, 375–383.

[9] Zhu, M. L.; Sun, Z. D.; Zhang, Z. X.; Shi, Q. F.; He, T. Y. Y.; Liu, H. C.; Chen, T.; Lee, C. Haptic-feedback smart glove as a creative human–machine interface (HMI) for virtual/augmented reality applications. *Sci. Adv.* **2020**, *6*, eaaz8693.

[10] Dinh, T.; Nguyen, T.; Phan, H. P.; Nguyen, T. K.; Dau, V. T.; Nguyen, N. T.; Dao, D. V. Advances in rational design and materials of high-performance stretchable electromechanical sensors. *Small* **2020**, *16*, 1905707.

[11] Guo, Y. J.; Wei, X.; Gao, S.; Yue, W. J.; Li, Y.; Shen, G. Z. Recent advances in carbon material-based multifunctional sensors and their applications in electronic skin systems. *Adv. Funct. Mater.* **2021**, *31*, 2104288.

[12] Liu, Z.; Xu, J.; Chen, D.; Shen, G. Z. Flexible electronics based on inorganic nanowires. *Chem. Soc. Rev.* **2015**, *44*, 161–192.

[13] Lee, S.; Reuveny, A.; Reeder, J.; Lee, S.; Jin, H.; Liu, Q. H.; Yokota, T.; Sekitani, T.; Isoyama, T.; Abe, Y. et al. A transparent bending-insensitive pressure sensor. *Nat. Nanotechnol.* **2016**, *11*, 472–478.

[14] Zhang, J. L.; Wang, M.; Yang, Z. H.; Zhang, X. H. Highly flexible and stretchable strain sensors based on conductive whisker carbon nanotube films. *Carbon* **2021**, *176*, 139–147.

[15] Zhou, X. Z.; Zhang, X.; Zhao, H. X.; Krishnan, B. P.; Cui, J. X. Self-healable and recyclable tactile force sensors with post-tunable sensitivity. *Adv. Funct. Mater.* **2020**, *30*, 2003533.

[16] Bi, P.; Liu, X. W.; Yang, Y.; Wang, Z. Y.; Shi, J.; Liu, G. M.; Kong, F. F.; Zhu, B. P.; Xiong, R. Silver-nanoparticle-modified polyimide for multiple artificial skin-sensing applications. *Adv. Mater. Technol.* **2019**, *4*, 1900426.

[17] Guan, F. Y.; Xie, Y.; Wu, H. X.; Meng, Y.; Shi, Y.; Gao, M.; Zhang, Z. Y.; Chen, S. Y.; Chen, Y.; Wang, H. P. et al. Silver nanowire-bacterial cellulose composite fiber-based sensor for highly sensitive detection of pressure and proximity. *ACS Nano* **2020**, *14*, 15428–15439.

[18] Zhang, H. Y.; Lowe, A.; Kalra, A.; Yu, Y. A flexible strain sensor based on embedded ionic liquid. *Sensors* **2021**, *21*, 5760.

[19] Wang, X. P.; Liu, X.; Bi, P.; Zhang, Y. Y.; Li, L. T.; Guo, J. R.; Zhang, Y.; Niu, X. F.; Wang, Y.; Hu, L. et al. Electrochemically enabled embedded three-dimensional printing of freestanding gallium wire-like structures. *ACS Appl. Mater. Interfaces* **2020**, *12*, 53966–53972.

[20] Yang, L.; Wang, R. Y.; Song, Q. T.; Liu, Y.; Zhao, Q. Q.; Shen, Y. F. One-pot preparation of porous piezoresistive sensor with high strain sensitivity via emulsion-templated polymerization. *Compos. Part A: Appl. Sci. Manuf.* **2017**, *101*, 195–198.

[21] Araromi, O. A.; Graule, M. A.; Dorsey, K. L.; Castellanos, S.; Foster, J. R.; Hsu, W. H.; Passy, A. E.; Vlassak, J. J.; Weaver, J. C.; Walsh, C. J. et al. Ultra-sensitive and resilient compliant strain gauges for soft machines. *Nature* **2020**, *587*, 219–224.

[22] Xu, W. J. H.; Hu, S. Y.; Zhao, Y.; Zhai, W.; Chen, Y. H.; Zheng, G. Q.; Dai, K.; Liu, C. T.; Shen, C. Y. Nacre-inspired tunable strain sensor with synergistic interfacial interaction for sign language interpretation. *Nano Energy* **2021**, *90*, 106606.
[23] Zhang, M. C.; Wang, C. Y.; Wang, H. M.; Jian, M. Q.; Hao, X. Y.; Zhang, Y. Y. Carbonized cotton fabric for high-performance wearable strain sensors. *Adv. Funct. Mater.* **2017**, *27*, 1604795.
[24] Yu, Y.; Luo, Y. F.; Guo, A.; Yan, L. J.; Wu, Y.; Jiang, K. L.; Li, Q. Q.; Fan, S. S.; Wang, J. P. Flexible and transparent strain sensors based on super-aligned carbon nanotube films. *Nanoscale* **2017**, *9*, 6716–6723.
[25] Cheng, Y.; Wang, R. R.; Sun, J.; Gao, L. A stretchable and highly sensitive graphene-based fiber for sensing tensile strain, bending, and torsion. *Adv. Mater.* **2015**, *27*, 7365–7371.
[26] Tang, N.; Zhou, C.; Qu, D. Y.; Fang, Y.; Zheng, Y. B.; Hu, W. W.; Jin, K.; Wu, W. W.; Duan, X. X.; Haick, H. A highly aligned nanowire-based strain sensor for ultrasensitive monitoring of subtle human motion. *Small* **2020**, *16*, 2001363.
[27] Wang, Z. Y.; Bi, P.; Yang, Y.; Ma, H. Y.; Lan, Y. C.; Sun, X. L.; Hou, Y.; Yu, H. Y.; Lu, G. X.; Jiang, L. M. et al. Star-nose-inspired multi-mode sensor for anisotropic motion monitoring. *Nano Energy* **2021**, *80*, 105559.
[28] Zhang, B. C.; Wang, H.; Zhao, Y.; Li, F.; Ou, X. M.; Sun, B. Q.; Zhang, X. H. Large-scale assembly of highly sensitive Si-based flexible strain sensors for human motion monitoring. *Nanoscale* **2016**, *8*, 2123–2128.
[29] Xu, W.; Yang, T. T.; Qin, F.; Gong, D. D.; Du, Y. J.; Dai, G. A sprayed graphene pattern-based flexible strain sensor with high sensitivity and fast response. *Sensors* **2019**, *19*, 1077.
[30] Luo, C. Z.; Jia, J. J.; Gong, Y. N.; Wang, Z. C.; Fu, Q.; Pan, C. X. Highly sensitive, durable, and multifunctional sensor inspired by a spider. *ACS Appl. Mater. Interfaces* **2017**, *9*, 19955–19962.
[31] Amjadi, M.; Pichitpajongkit, A.; Lee, S.; Ryu, S.; Park, I. Highly stretchable and sensitive strain sensor based on silver nanowire-elastomer nanocomposite. *ACS Nano* **2014**, *8*, 5154–5163.
[32] Ou, Y.; Zhao, T. T.; Zhang, Y.; Zhao, G. H.; Dong, L. J. Stretchable solvent-free ionic conductor with self-wrinkling microstructures for ultrasensitive strain sensor. *Mater. Horiz.* **2022**, *9*, 1679–1689.
[33] Wang, Q.; Ling, S. J.; Liang, X. P.; Wang, H. M.; Lu, H. J.; Zhang, Y. Y. Self-healable multifunctional electronic tattoos based on silk and graphene. *Adv. Funct. Mater.* **2019**, *29*, 1808695.
[34] Lu, N. S.; Lu, C.; Yang, S. X.; Rogers, J. Highly sensitive skin-mountable strain gauges based entirely on elastomers. *Adv. Funct. Mater.* **2012**, *22*, 4044–4050.
[35] Hempel, M.; Nezich, D.; Kong, J.; Hofmann, M. A novel class of strain gauges based on layered percolative films of 2D materials. *Nano Lett.* **2012**, *12*, 5714–5718.
[36] Chao, M. Y.; Wang, Y. G.; Ma, D.; Wu, X. X.; Zhang, W. X.; Zhang, L. Q.; Wan, P. B. Wearable MXene nanocomposites-based strain sensor with tile-like stacked hierarchical microstructure for broad-range ultrasensitive sensing. *Nano Energy* **2020**, *78*, 105187.
[37] Yang, Y. N.; Cao, Z. R.; He, P.; Shi, L. J.; Ding, G. Q.; Wang, R. R.; Sun, J. $Ti_3C_2T_x$ MXene-graphene composite films for wearable strain sensors featured with high sensitivity and large range of linear response. *Nano Energy* **2019**, *66*, 104134.
[38] Chen, Y.; Zhang, Y. Y.; Song, F.; Zhang, H. Y.; Zhang, Q. K.; Xu, J.; Wang, H. P.; Ke, F. Y. Graphene decorated fiber for wearable strain sensor with high sensitivity at tiny strain. *Adv. Mater. Technol.* **2021**, *6*, 2100421.
[39] Wang, C. Y.; Xia, K. L.; Jian, M. Q.; Wang, H. M.; Zhang, M. C.; Zhang, Y. Y. Carbonized silk georgette as an ultrasensitive wearable strain sensor for full-range human activity monitoring. *J. Mater. Chem. C* **2017**, *5*, 7604–7611.
[40] Wang, C. Y.; Xia, K. L.; Zhang, M. C.; Jian, M. Q.; Zhang, Y. Y. An all-silk-derived dual-mode e-skin for simultaneous temperature-pressure detection. *ACS Appl. Mater. Interfaces* **2017**, *9*, 39484–39492.
[41] Wang, Q.; Jian, M. Q.; Wang, C. Y.; Zhang, Y. Y. Carbonized silk nanofiber membrane for transparent and sensitive electronic skin. *Adv. Funct. Mater.* **2017**, *27*, 1605657.